A particle method strategy for the simulation of AE statistics indisordered materials

A particle method strategy for the simulation of AE statistics in disordered materials

Stefano Invernizzi[1], Giuseppe Lacidogna[1], Alberto Carpinteri [1]

[1]*Dipartimento di Ingegneria Strutturale e Geotecnica, Politecnico di Torino, Italy*
E-mail: stefano.invernizzi@polito.it, giuseppe.lacidogna@polito.it, alberto.carpinteri@polito.it,

SUMMARY. We present some numerical simulations of AE due to damage propagation in disordered materials under compression and bending. To this purpose, the AE cumulative number, the time frequency analysis and the statistical properties of AE time series will be numerically simulated adopting the so-called "particle method strategy" [1]. The method provides the velocity of particles in a set simulating the behavior of a granular system and, therefore, is suitable to model the compressive wave propagation and acoustic emission (corresponding to cracking) in a solid body. The numerical simulations [2] correctly describe the compression test in terms of mean stress-strain response and crack pattern [3]. The size effects on the peak compressive strength and on the AE count are correctly reproduced. In addition, the amplitude distribution (*b*-value) and temporal evolution of AE events due to cracking, crucial for the evaluation of damage and remaining lifetime, were simulated and result in agreement with the experimental evidences.

1 INTRODUCTION

Instrumental and nondestructive investigation methods are currently employed to measure and check the evolution of adverse structural phenomena, such as damage and cracking, and to predict their subsequent developments. The choice of a technique for controlling and monitoring reinforced concrete or masonry structures is strictly correlated with the kind of structure to be analyzed and the data to be extracted [4,5].

This study first addresses the pure compression test carried out in the laboratory and performed on drilled concrete cores obtained from two pilasters sustaining a viaduct along an Italian highway [6]. At the same time, the cracking process taking place during the test was monitored using the acoustic emission (AE) technique. A similar approach has been already exploited in [7] attempting to link the amount of AE with the structural deflections.

In the assessment of structural integrity, the AE technique has proved particularly effective [7-9], in that it makes it possible to estimate the amount of energy released during the fracture process and to obtain information on the criticality of the process underway. Strictly connected to the energy detected by AE is the energy dissipated by the monitored structure. The energy dissipated during crack formation in structures made of quasi-brittle materials plays a fundamental role in the behavior throughout their entire life. Recently, according to fractal concepts, an ad hoc method has been employed to monitor structures by means of the AE technique [6-9]. The fractal theory takes into account the multiscale character of energy dissipation and the strong size effects associated with it. With this energetic approach, it becomes possible to introduce a useful damage parameter for structural assessment based on a correlation between AE activity in the structure and the corresponding activity recorded on specimens of different sizes, tested to failure by means of

pure compression tests. Finally, some preliminary results are shown also about the three-point bending configuration. The main achievement of the present work consists in showing how the amount of cracking obtained from the numerical simulation and the experimentally detected AE events share the same dimensional and temporal scaling laws.

2 COMBINED COMPRESSION AND AE TESTS

By means of the AE technique, we analyzed the damage evolution in two pilasters sustaining a viaduct along an Italian highway built in the 1950s. From the pilasters we drilled some concrete cylindrical specimens in order to detect the mechanical properties of the material under compression and to evaluate the scale effects in size and time on AE activity [6].
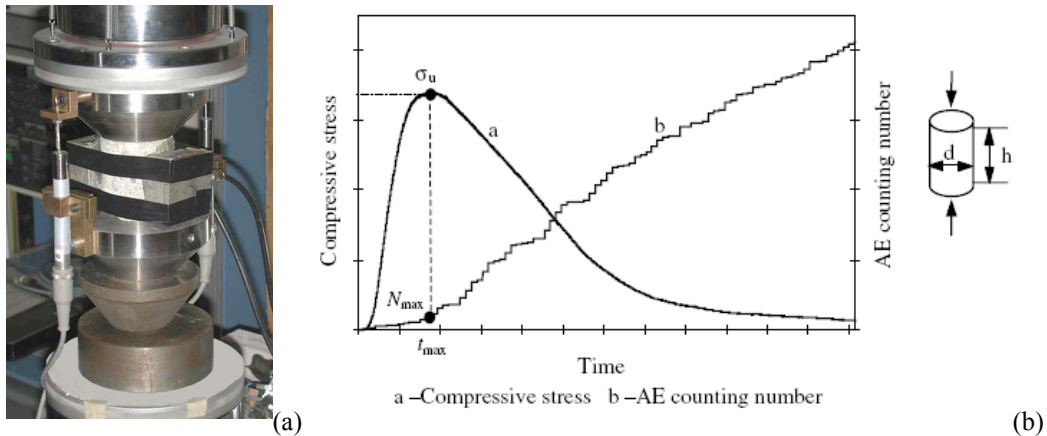

Figure 1: Apparatus adopted for compression tests (a); Stress and cumulated event number versus time (b).

2.1 Test specimens and testing equipment

The cementitious material, of rather good mechanical characteristics, presents an apparent specific weight of 2.22 g/cm^3 and a maximum aggregate size of 15 mm. For each pilaster, three different specimen diameters d are considered in a maximum scale range of 1:3.4. The specimens present three different slendernesses: λ = h/d = 0.5, 1.0 and 2.0, with d equal to 27.7, 59, 94 mm, respectively. For each of these nine geometries, three specimens have been tested, for a total of 54 cases (two pilasters). The average values obtained from the experimental data of pilaster P1 are reported in Table 1. The system adopted in the compression test utilizes rigid steel platens, the lateral deformation of concrete being therefore confined at the specimen ends, which are forced to have the same lateral deformation as the rigid platens (Figure 1a). The stress and cumulated event number versus time for a specimen of intermediate size is represented in Figure 1b. The critical number of AE cumulative events N_{max} is represented in correspondence to the peak stress σ_u. Similar results were observed in the other cases.

3 PARTICLE SIMULATIONS

The simulations have been carried out with ESyS-Particle, an open source implementation of the Distinct Element Method [1]. ESyS-Particle has been developed in-house within the Earth Systems Science Computational Centre (ESSCC) at the University of Queensland [10] since 1994.

Table 1: Experimental values obtained on concrete samples from pilaster P1.

Specimen Type	Diameter d [mm]	Slenderness $\lambda=h/d$	Experimental peak stress [Mpa]	N_{max} at σ_u	Numerical peak stress [Mpa]
C11	27.7	0.5	91.9	1186	77.5
C12	27.7	1.0	62.8	1191	61.7
C13	27.7	2.0	48.1	1188	34.7
C21	59.0	0.5	68.1	8936	101.4
C22	59.0	1.0	53.1	8934	36.6
C23	59.0	2.0	47.8	8903	26.3
C31	94.0	0.5	61.3	28502	66.4
C32	94.0	1.0	47.8	28721	33.3
C33	94.0	2.0	44.1	28965	31.8

The simulation is based on direct integration of the Newton's motion equations with the Verlet algorithm. The normal interaction between colliding particles is linear and proportional to the particle small overlapping, whereas Coulomb friction, with both static and dynamic friction coefficients, rules the tangential interaction. In addition, bonded links are established between neighbor particles, according to the scheme in Figure 2a. The bonded link is elastic perfectly brittle. The rupture of the bond is based on a fracture criterion that accounts for the axial, shear, torsion and bending behavior. The particles are filled together with the random packing algorithm LSMGenGeo [11], on the base of the maximum and minimum particle radius, which in our case correspond respectively to the maximum and minimum concrete aggregate radius (i.e. r_{max}=7.5 *mm*, r_{min}=1.5 *mm*).
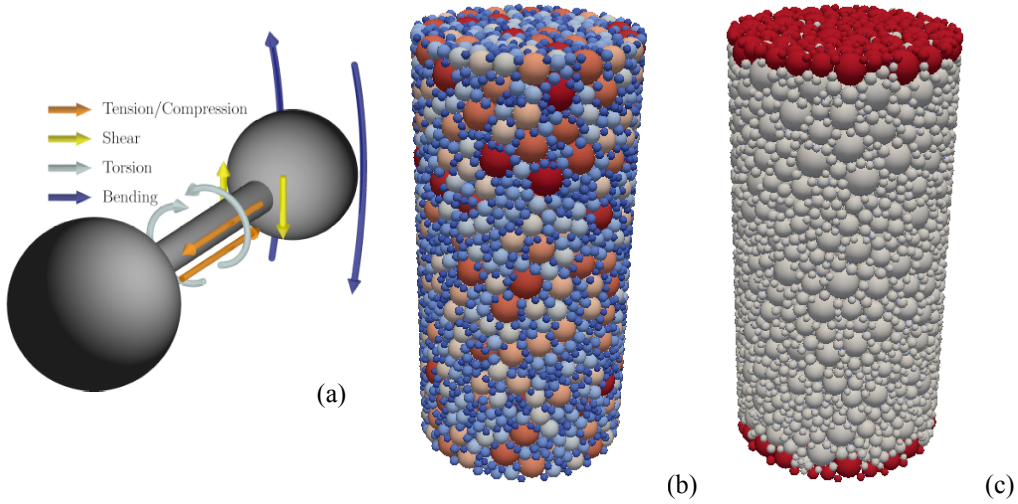

Figure 2: Scheme of the bonded interaction between two particles (a); view of the specimen particle size distribution (colors indicate different diameters) (b); detail of the particles (in red) bonded to the loading platen (c).
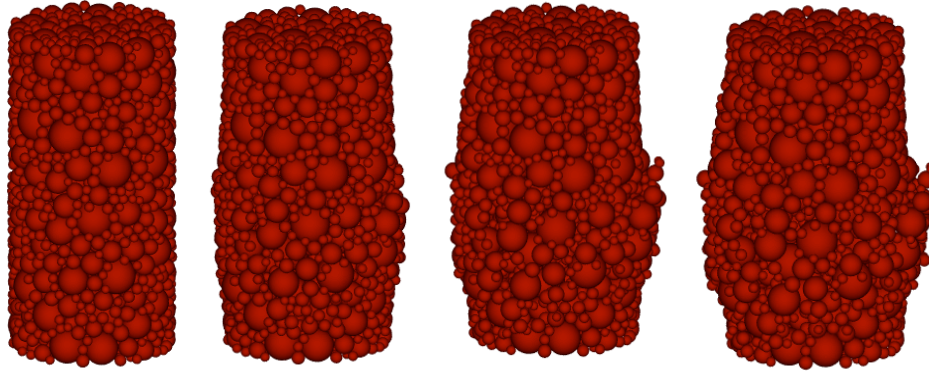
Figure 3: Evolution of specimen crushing during the simulated compression test (sample C23).

An exclusion method provides that once the bonded link is broken, the frictional interaction takes place between the neighbor particles. When the maximum and minimum radius of particles are quite different, experience shows that a power-law size distribution is obtained, providing a good approximation of the actual concrete aggregate size distribution. The load is applied to the specimen by means of moving planes. In order to simulate perfect friction between the loading platen and the specimens, the particles closer to the platens were bonded to the moving planes. In Figure 2c, bonded particles of the specimen are shown in red. The larger specimen was made of almost 9000 particles. In the present study, special attention was paid to the simulation of the scaling of the mechanical response, rather than to provide a detailed interpretation of a specific set of tests. Nevertheless, the mechanical parameters adopted in the analysis were chosen to better interpolate the experimental strength in the whole dimensional range.

The simulations are carried out at a fixed strain velocity equal to $10^{-4}s^{-1}$. In this way the duration of each simulation is independent of the specimen size, and it is possible to adopt a unique time integration step equal to 0.04 s. A viscous type damping, proportional to the particle velocity is introduced in the simulation. The choice of the damping coefficient (in our case equal to 0.02) is based on the minimum value that regularizes the simulation without affecting the stress-strain behavior.

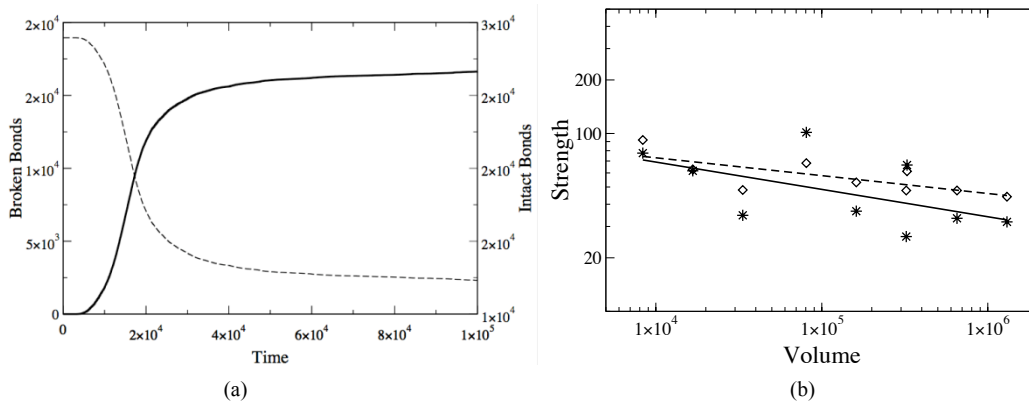(a)   (b)

Figure 4: Cumulative distribution of broken (continuous line) and intact (dashed line) bonds for increasing time (a). Comparison between experimental size effect on compression strength (diamonds and dotted line) and numerical results (stars and continuous line) (b).

The position and velocity of each particle during the simulation can be recorded at a certain integration time. The cracking and crushing pattern of the specimen is shown in Figure 3 for specimen C23. During the first stage of loading, the specimen barrels. Soon after, the bonds of the central region are broken, diagonal cracks propagate and splitting mechanisms or even the explosion of the sample can take place.

The bearing load is obtained from the integration of the contact forces exchanged with the loading platens, while the position of the platens allows for the calculation of the strain. Figure 4a shows the evolution of the broken and intact bonded links number during the simulation (C33). In the very initial stage the number of intact bonds is constant, corresponding to the linear elastic regime. The damage starts rather before the peak load and propagates slowly at the beginning, with an increasing number of broken bonds. At the peak load the damage spreads across the sample very rapidly, corresponding to a quite brittle behavior and a sudden drop in the number of intact bonds.

Finally, Figure 4b shows the bilogarithmic diagram of the peak load versus the specimen volume. The experimental values (diamonds) are aligned on a straight dashed line with slope equal to −0.10. The simulation results (stars) are aligned on a straight continuous line with slope equal to −0.15. The particle numerical simulation is able to describe correctly the trend of the size effect on the compression strength, being in rather good agreement with experimental results.

4 COMPARISON BETWEEN NUMERICAL AND EXPERIMENTAL AE SCALING

In previous works [6-8], a statistical and fractal analysis of data from laboratory experiments was performed, considering the multiscale aspect of cracking phenomena. The fractal approach captures the multiscale character of energy dissipation and the strong size effects associated with it. This makes it possible to introduce a useful energy-related parameter for the damage determination in full-size structures, by comparing the AE monitoring results with the values obtained on a reference specimen sampled from the structure and tested up to failure. This approach has been exploited by the authors also for the interpretation of double flat-jack tests performed in historical masonry walls [12].

Fragmentation theories have shown that, during microcrack propagation, energy dissipation occurs in a fractal domain comprised between a surface and the specimen volume V [13,14]. This implies that a fractal energy density (having anomalous physical dimensions):

$$\Gamma = \frac{W_{\max}}{V^{D/3}},$$

(1)

can be considered as the size-independent parameter. In the fractal criterion of Eq. (1), $W_{\max}$ = total dissipated energy; Γ = fractal energy density; and D = fractal exponent comprised between 2 and 3.

On the other hand, during microcrack propagation, acoustic emission events can be clearly detected. Since the energy dissipated, W, is proportional to the number of the oscillations counts N related to the AE events, Γ_{AE} can be considered as a size-independent parameter:

$$\Gamma_{AE} = \frac{N_{\max}}{V^{D/3}},$$

(2)

where Γ_{AE} = fractal acoustic emission event density; and $N_{\max}$ is evaluated at the peak stress, σ_u. Eq. (2) predicts a volume effect on the maximum number of AE events for a specimen tested up to the peak stress.

The extent of structural damage in a full-size structure can be worked out from the AE data recorded on a reference specimen (subscript r) obtained from the structure. From Eq. (2) we get:

$$N_{\max} = N_{\max,r}\left(\frac{V}{V_r}\right)^{D/3} , \qquad (3)$$

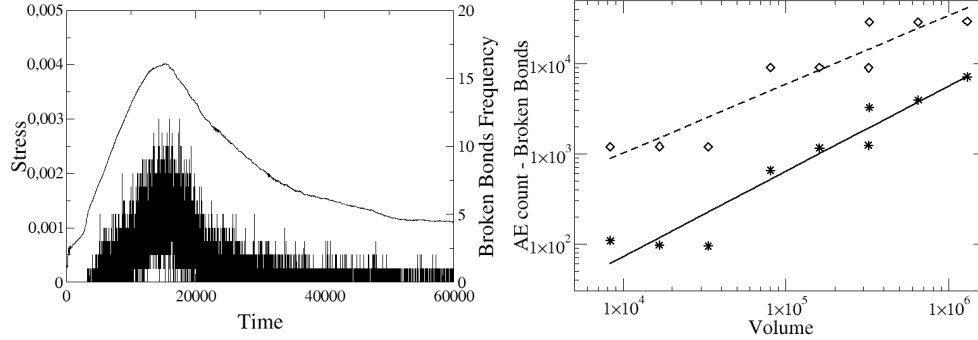from which we can obtain the structure critical number of AE events $N_{\max}$.

Figure 5: Frequency of broken bonds during the compression test C33 (a); comparison between experimental size effect on AE counts (diamonds and dotted line) and numerical simulations (stars and dotted line) and numerical simulations (stars and continuous line) (b).

In order to provide a numerical interpretation to the AE phenomenon, the AE counting is put in direct comparison with the number of broken bonds at a certain time. More in detail, each event is composed of the number of bonds broken in a time interval equal to four time integration steps (i.e. equal to 0.16 *s*), while the magnitude is proportional to the number of broken bonds. This simple assumption implies that each bond releases the same energy at rupture, each bond being assigned the same strength. More detailed analogies have been presented in the literature (e.g. [15]), which are required for the definition of a localization and clustering criterion for the events.

The frequency and magnitude of simulated events are shown in Figure 5a, compared with the evolution of the mean stress in the sample. In the elastic initial stage no emissions are recorded, since the specimen is undamaged. Afterwards, the frequency of high magnitude events gradually increases. After the peak load, a quite rapid decrease of events is recorded, in good agreement with the experimental evidence of the AE events.

Figure 5b shows the bilogarithmic diagram of the experimental AE count (diamonds) and of the broken bonds (stars) at the peak load versus the specimen volume. This diagram emphasizes the size effect on the AE (dashed straight line) with an exponent equal to 0.76, which corresponds well with the numerical size effect on broken bonds (continuous straight line) with an exponent equal to 0.90.

4.1 *AE frequency–magnitude statistics*

Since the studies of Mogi and Scholz [16,17] on AE, we know that the Gutenberg-Richter empirical law can be observed at the laboratory sample scale. They showed that a significant overlap exists between the definition of AE and earthquake. This is further reinforced by the evidence that brittle fracture obeys similar statistics from tectonic earthquakes to the dislocation movements smaller than micron size [18]. Moreover, in recent years, experiments employing

acoustic emission have established remarkable results concerning the model of process zone and the quasistatic fault growth [19]. Such experiment-based knowledge is expected to be useful for studying the fundamental behavior of natural earthquakes, because it is widely accepted that fault systems are scale-invariant [20, 21] and there exist universal similarities between faulting behaviors, from small-scale microcracking to large-scale seismic events. For example, AE events caused by microcracking activity [16,19-21] and stick-slip along a crack plane [23, 24] are similar to those generated by natural earthquakes.

By analogy with seismic phenomena, in the AE technique the magnitude may be defined as follows [14,25-26]:

$$m = \text{Log}\, A_{\text{max}} + f(r), \tag{4}$$

where A_{max} is the amplitude of the signal espressed in μV and $f(r)$ is a correction coefficient whereby the signal amplitude is taken to be a decreasing function of the distance r between the source and the AE sensor. In seismology, the Gutenberg-Richter empirical law [27]:

$$\text{Log}\, N(\geq m) = a - bm, \tag{5}$$

expresses the relationship between magnitude and total number of earthquakes in any given region and time period, and is the most widely used statistical relation to describe the scaling properties of seismicity. In Eq. (5), N is the cumulative number of earthquakes with magnitude $\geq m$ in a given area and within a specific time range, while a and b are positive constants varying from a region to another and from a time interval to another. Eq. (5) has been used successfully in the AE field to study the scaling laws of AE wave amplitude distribution. This approach evidences the similarity between structural damage phenomena and seismic activities in a given region of the Earth, extending the applicability of the Gutenberg-Richter law to structural engineering.
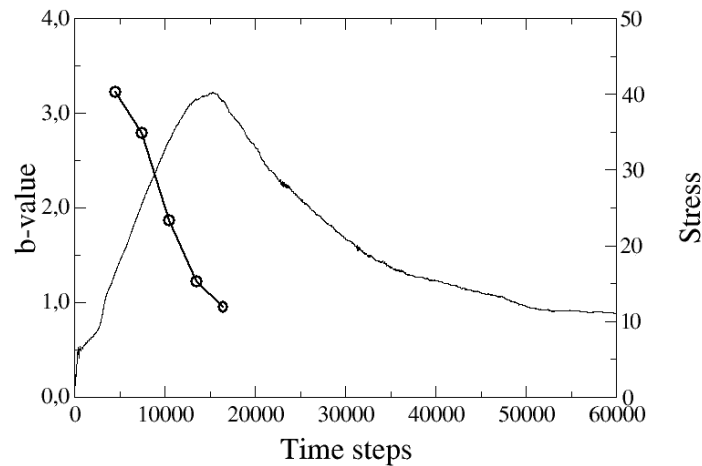

Figure 6: Evolution of the simulated *b*-value (circles) with time compared with the stress level.

According to Eq. (5), the *b*-value changes systematically at different times in the course of the damage process and therefore can be used to estimate damage evolution modalities [14,25]. For sample C33, the analysis of the *b*-value during the compression test was carried out. The *b*-values,

computed for non-overlapping subsequent time windows of 120 s (i.e. 3000 time steps), are reported together with the stress curve. In other words, the *b*-values are determined during the tests by taking into account only current values. With this method, already adopted in other works on the damage analysis of structural concrete elements [25], the simulation time was subdivided into 6 intervals up to 720 s (i.e. 18000 time steps). The first time window has no events, since the specimen is in the linear regime, thus the *b*-value is not calculated. In Figure 7, the final *b*-value approaches to one for sample C33 [26]. Figure 6 also shows that AE generated during the early stages of loading implies an high *b*-value > 1.5. In particular, the *b*-value obtained for sample C33 results to be greater than 3.0 immediately after the beginning of the test, it reaches the value 1.5 just before the peak stress and finally tends to 1.0 at the peak stress [28].

5 GUTEMBERG-RICTER STATISTICS OF THREE POINT BENDING TEST

A two-dimensional simulation of three-point bending test and AE acquisition [12] has also been performed. The particle discretization was limited to the central region of the beam, where almost uniform bending was simulated imposing the rotation of the extreme sections (shown in red in Figure 7a). The initial notch is obtained removing the corresponding bonds. As soon as the bonds between particles reach the failure limit, they are removed, and the crack proceeds to the extrados of the beam (Figure 7b).
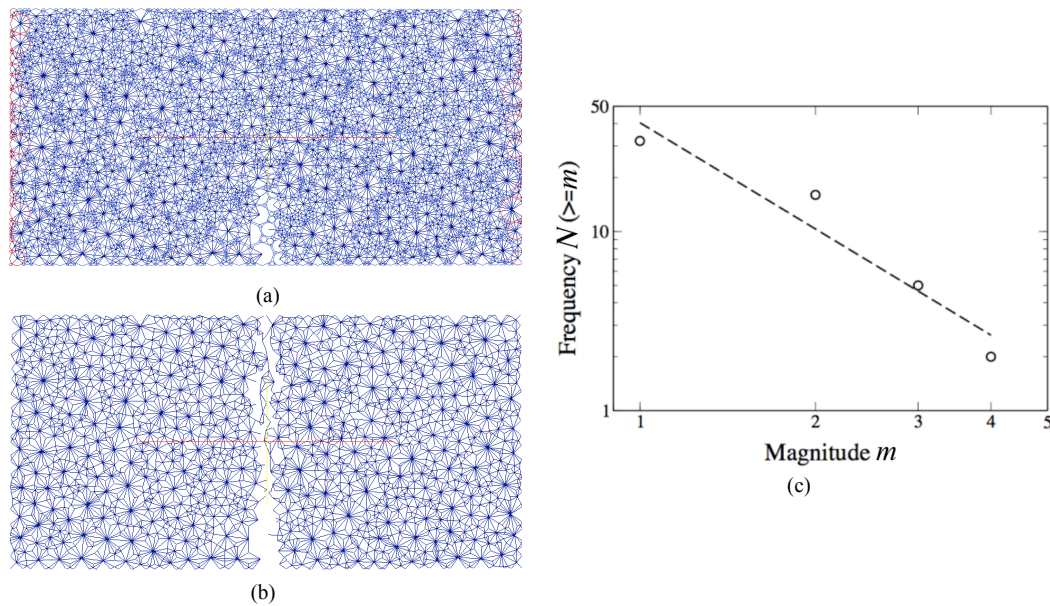

(a)

(b)

(c)

Figure 7: Initial configuration (a); final configuration (b); frequency magnitude bilinear diagram: *a*=40.4, *b*=1.97 (c).

Analogously to the assumption adopted in the compression test, the magnitude of each event is obtained summing up the number of bonds broken in each non-overlapping time window, in this case equal to 300 time steps. Finally, the frequency of the magnitude events that overcame a certain value *m* is reported in the classical Gutember-Richter chart (Figure 7c). It is worth noting that, in agreement with the experimental acquisition [14], the computed frequencies are aligned on a straight line. The slope of this line, which corresponds to the *b* value, is higher than the

experimental value, and equal to 1.97. Further analyses are necessary to investigate the effect of the simulation dimensionality, and to obtain a better parameter calibration of the model.

6 CONCLUSIONS

A numerical simulation of a concrete compression test combined with acoustic emission monitoring has been proposed. The numerical results agree rather satisfactorily with the experimental evidences, and the crack patterns are simulated correctly. The model is able to describe the decrease in the overall strength with increasing size. In addition, the number of acoustic emissions is put into relation with the number of broken bonds at the peak stress. A good correlation is found between the amount of cracking simulated numerically and the experimental acoustic emission counting for different specimen sizes. In addition, the amplitude distribution (b-value) and temporal evolution of AE events due to cracking, crucial for the evaluation of damage and remaining lifetime, have been simulated in good agreement with the experimental data.

Finally, some preliminary results about the simulation of the AE statistics in the three-point bending test are reported. We obtained a good qualitative simulation of the Gutember-Richter law, although further analyses are necessary to investigate the effect of the simulation dimensionality, and to obtain a better parameter calibration of the model.

7 ACKNOWLEDGEMENTS

References
[1] Cundall P.A., "A computer model for simulating progressive large scale movements in blocky rock systems", in *Proceedings ISRM Symp., Nancy, France*, **2**, 129-136 (1971).
[2] Abe S., Place D., Mora P. "A parallel implementation of the lattice solid model for the simulation of rock mechanics and earthquake dynamics". *Pure Appl Geophys*; **161**, 2265-77 (2004).
[3] Invernizzi S., Lacidogna G., Manuello A., Carpinteri A,. "Numerical simulation of AE activity in quasi-brittle materials under compression", in *Proceedings of the SEM Annual Conference, Society for Experimental Mechanics Inc. (USA), SEM Annual Conference*, Indianapolis, Indiana USA June 7-10, (2010).
[4] A. Carpinteri, P. Bocca, *Damage and Diagnosis of Materials and Structures*, Pitagora Editrice, Bologna, Italy. (1991).
[5] A. Anzani, L. Binda, G. Mirabella Roberti, "The effect of heavy persistent actions into the behavior of ancient masonry", *Materials & Structures*, **33**, 251-261 (2000).
[6] A. Carpinteri, G. Lacidogna, N. Pugno, "Structural damage diagnosis and life-time assessment by acoustic emission monitoring", *Engineering Fractures Mechanics*, **74**, 273-289 (2007).
[7] A. Carpinteri, S. Invernizzi, G. Lacidogna, "Structural assessment of a XVIIth century masonry vault with AE and numerical techniques", *International Journal of Architectural Heritage*, **1**(2), 214-226 (2007).
[8] A. Carpinteri, G. Lacidogna, "Structural monitoring and integrity assessment of medieval towers", *Journal of Structural Engineering (ASCE)*, **132**, 1681-1690 (2006).
[9] A. Carpinteri, G. Lacidogna, "Damage monitoring of a masonry building by the acoustic emission technique", *Materials & Structures*, **39**, 161-167 (2006).

[10] https://twiki.esscc.uq.edu.au/bin/view/ESSCC/ParticleSimulation

[11] https://launchpad.net/esys-particle/

[12] A. Carpinteri, S. Invernizzi, G. Lacidogna, "Historical brick-masonry subjected to double flat-jack test: Acoustic Emissions and scale effects on cracking density", *Construction and Building Materials*, **23**(8), 2813-2820, (2009).

[13] A. Carpinteri, N. Pugno, "A multifractal comminution approach for drilling scaling laws", *Powder Technology*, **131**(1), 93-98, (2003).

[14] Carpinteri, A., Lacidogna, G., Niccolini, G., Puzzi, S. "Critical defect size distributions in concrete structures detected by the acoustic emission technique", *Meccanica*, **43**, 349–363, (2008).

[15] J.F. Hazzard, R.P. Young, "Simulating acoustic emissions in bonded-particle models of rock", *International Journal of Rock Mechanics in Mining Science*, **37**, 867-872, (2000).

[16] Mogi, K. "Magnitude frequency relations for elastic shocks accompanying fractures of various materials and some related problems in earthquakes", *Bull. Earthquake Res. Inst. Univ. Tokyo*, **40**, 831-853, (1962).

[17] Scholz, C. H. "The frequency-magnitude relation of microfracturing in rock and its relation to earthquakes", *Bull. Seismol. Soc. Am.,* **58**, 399-415, (1968).

[18] M.C. Miguel, A. Vespignani, S. Zapperi, J. Weiss, J.R. Grasso, "Intermittent dislocation flow in viscoplastic deformation", *Nature*, **410**, 667-670 (2001).

[19] D.A. Lockner, J.D. Byerlee, V. Kuksenko, A. Ponomarev, A. Sidorin, "Quasi static fault growth and shear fracture energy in granite", *Nature* **350**, 39-42 (1991).

[20] T. Hirata, "Fractal dimension of fault system in Japan: fracture structure in rock fracture geometry at various scales", *Pure Appl. Geophys*. **131**, 157-170 (1989).

[21] E. Bonnet, O. Bour, N.E. Odling, P. Davy, I. Main, P. Cowie, B. Berkowitz, "Scaling of fracture systems in geological media", *Rev. Geophys*. **39**, 347-383 (2001).

[22] X.Lei, "How do asperities fracture? An experimental study of unbroken asperities", *Earth Planet. Sci. Lett.* **213**, 347-359 (2003).

[23] N. Kato, K. Yamamoto, T. Hirasawa, "Microfracture processes i the break down zone during dynamic shear rupture inferred from laboratory observation of near-fault high-frequency strong motion", *Pure Appl. Geophys*. **142**, 713-734 (1994).

[24] X.L. Lei, O. Nishizawa, K. Kusunose, A. Cho, T. Satoh, "On the compressive failure of shale samples containing quartz-healed joints using rapid AE monitoring: the role of asperities", *Tectonophysics* **328**, 329-340 (2000).

[25] S. Colombo, I.G. Main, M.C. Forde, "Assessing damage of reinforced concrete beam using ''b-value'' analysis of acoustic emission signals", *J. Mat. Civil Eng. (ASCE)* **15**, 280-286 (2003).

[26] M.V.M.S. Rao, P.K.J. Lakschmi, "Analysis of b-value and improved b-value of acoustic emissions accompanying rock fracture", *Curr. Sci. – Bangalore* **89**, 1577–1582 (2005).

[27] C.F. Richter, *Elementary Seismology*. W.H. Freeman, San Francisco, CA; and London. (1958)

[28] A. Carpinteri, G. Lacidogna, A. Manuello, "The *b*-value analysis for the stability investigation of the ancient Athena temple in Syracuse", *Strain*, doi:10.1111/j.1475-1305.2008.00602.x (2009).